

Observation of Locked Phase Dynamics and Enhanced Frequency Stability in Synchronized Micromechanical Oscillators

Deepak K. Agrawal, Jim Woodhouse, and Ashwin A. Seshia*

Department of Engineering, University of Cambridge, Cambridge CB2 1PZ, United Kingdom
(Received 21 March 2013; revised manuscript received 13 May 2013; published 20 August 2013)

Even though synchronization in autonomous systems has been observed for over three centuries, reports of systematic experimental studies on synchronized oscillators are limited. Here, we report on observations of internal synchronization in coupled silicon micromechanical oscillators associated with a reduction in the relative phase random walk that is modulated by the magnitude of the reactive coupling force between the oscillators. Additionally, for the first time, a significant improvement in the frequency stability of synchronized micromechanical oscillators is reported. The concept presented here is scalable and could be suitably engineered to establish the basis for a new class of highly precise miniaturized clocks and frequency references.

DOI: [10.1103/PhysRevLett.111.084101](https://doi.org/10.1103/PhysRevLett.111.084101)

PACS numbers: 05.45.Xt, 06.30.Ft, 84.30.Ng, 85.85.+j

The phenomenon of synchronization is widely observed in a variety of scientific contexts. Examples of synchronization can be found in various physical domains such as the coupled out-of-phase motion of pendulum clocks [1,2], multiorder synchronization in a magnetic resonance laser [3], rhythmic flashes of light pulses in fireflies [4], and the biological clock in humans, animals, and plants [5]. These apparently disparate systems are linked by a common thread that relates to the adjustment of rhythms in the presence of a weak coupling force, resulting in a frequency entrainment of these coupled self-sustained oscillators. Synchronized oscillators are associated with frequency entrainment and phase locking behavior.

There has been much recent interest in observations of synchronization in micro- and nanomechanical oscillators due to several practical applications [6–10]. However, experimental observations of synchronization at these length scales have been limited to the observation of frequency entrainment either in externally driven micromechanical resonators [11] or in laser driven optomechanical oscillators [12,13]. Moreover, the employed transduction schemes and coupling arrangements in these topologies result in additional complexities and limit scalability and chip-scale system integration. In this Letter, for the first time, we report the coupled frequency and phase dynamics of electrically coupled autonomous micromechanical oscillators with physical insight into system parameters governing the observation of synchronized response. Two electrostatically driven double-ended tuning-fork (DETF) silicon microresonators are utilized as the frequency determining elements for two independent oscillators that are then electrically coupled to observe a synchronized response.

An optical micrograph of the resonators is shown in Fig. 1(a). Each resonator is excited electrostatically in the out-of-phase in-plane flexural mode using a dc bias (V_{dc}) and an ac (v_{ac}) voltage, applied to the driving

electrode (see the Supplemental Material [14]). This results in a time varying capacitance across the electrodes which transforms the dynamic displacement to an output current (I) [15]. A parallel-plate capacitor situated between the two resonators couples the motional currents.

The open-loop response of the resonators is recorded using a network analyzer (Agilent 4396B) at several dc and ac voltages. Measurements are conducted at room temperature in a custom vacuum chamber at a pressure of approximately ≈ 50 mtorr. The measured frequency response in the linear regime is shown in Fig. 1(b). For similar bias and operating conditions, the average mismatch in the resonance frequencies is ≈ 440 Hz, arising due to manufacturing variations inherent to the fabrication process. The inherent dependence of the resonance frequency on V_{dc} in electrostatically transduced microelectromechanical systems (MEMS) resonators is seen to follow a well-established voltage tuning behavior [16]. The effect of v_{ac} on the frequency response is shown in Fig. 1(c). An increase in v_{ac} results in a large dynamic displacement which thereby increases the impact of the nonlinear restoring force on the resonance frequency, resulting in an amplitude-frequency (a - f) dependence. Moreover, for the given topology, mechanical nonlinearities harden the resonator and increase the resonance frequency while electrical nonlinearities are softening in nature, resulting in a reduction in the resonance frequency [17]. The cubic nonlinearity in the restoring force is also commonly associated with the Duffing bifurcation [18].

Next, each DETF resonator is embedded within the feedback loop of distinct board-level oscillator circuits. Each oscillator circuit comprises of a transimpedance amplifier, bandpass filter, and comparator. This oscillator architecture has been previously discussed elsewhere (see the Supplemental Material [14]) [19]. In this closed-loop configuration, the resonator is driven by the signal fed back to the driving electrode from the output of the comparator.

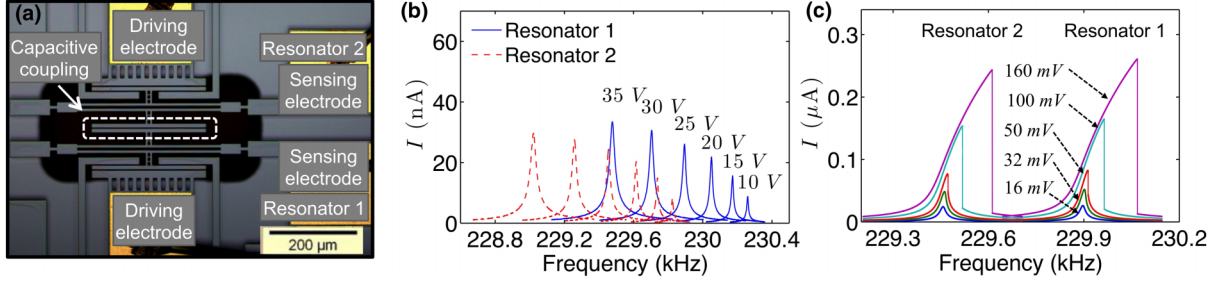


FIG. 1 (color online). Coupled silicon DETF micromechanical resonators. (a) An optical micrograph of the device fabricated in a commercial foundry process using a standard silicon-on-insulator MEMS process. (b) The linear frequency response is plotted at several V_{dc} voltages and at a fixed v_{ac} of 16 mV. In these responses, a reduction in the resonance frequency is a function of dc voltage results due to a reduction in the stiffness of the resonator. This characteristic can be used to reduce the frequency mismatch between the resonators. (c) The nonlinear response is plotted at several v_{ac} voltages and at a fixed 25 V V_{dc} voltage. At higher excitation levels, the resonant response skews towards the right, eventually exhibiting the Duffing bifurcation.

This feedback signal amplitude (V_F) is regulated using a potential divider arrangement. An increase in V_F increases the motional amplitude of the resonator and hence the a - f dependency via cubic nonlinearities.

The coupled dynamics of the discussed oscillator can be described using [14]

$$\begin{aligned} \ddot{I}_{1,2} + \omega_{o,2}^2 I_{1,2} + \mu_{1,2} \dot{I}_{1,2}^3 + \alpha_{1,2} \dot{I}_{1,2} - \beta_{1,2} \text{sgn}(\dot{I}_{1,2}) \\ + D_{1,2}(I_{1,2} - I_{2,1}) = 0. \end{aligned} \quad (1)$$

In Eq. (1), the first two terms represent a linear oscillator with natural frequency ω_o while μ , α , β , and $D_{1,2}$ represent the cubic nonlinearity of the resonator, positive linear damping of the resonator, negative damping regulated by the comparator output, and the strength of the current coupling, respectively. These equations can be solved numerically to assess the effects of V_F and V_{dc} on the coupled oscillator dynamics (see the Supplemental Material [14]).

During experiments, when both the oscillators are operated simultaneously, the coupling force is governed by the coupling capacitance and the difference of the motional currents. If the frequencies of the coupled oscillators are denoted as F_1 and F_2 and the mismatch as $\Delta F = F_1 - F_2$, frequency entrainment is achieved when $\Delta F = 0$ [5]. The corresponding frequency locking range is $\Delta f = f_1 - f_2$, where f_1 and f_2 are the output frequencies of the uncoupled oscillators, a condition in which only one oscillator is operated at a time. The applied dc bias voltages for each resonator are denoted as V_{dc_1} and V_{dc_2} , respectively.

The output response of the oscillators is observed using a spectrum analyzer (Agilent 4396B) and an oscilloscope simultaneously, and measurements are made when the oscillators exhibit stable limit-cycle behavior. Because of the capacitive coupling between the oscillators, the responses of each oscillator may be observed from the output port of the other. Initially, V_F is limited to 16 mV and a 15 V dc bias is applied to each oscillator, resulting in coupled steady-state limit-cycle responses. Consequently, ΔF (≈ 440 Hz) is reduced by varying V_{dc_1} from 15 to 35 V

while maintaining V_{dc_2} at 15 V. However, under such conditions, entrainment is not observed. This is potentially due to the employed nature of coupling and the underlying coupled oscillator dynamics. When two oscillators are coupled reactively, entrainment is achieved only when the amplitude and frequency response are correlated through a nonlinear mechanism. This is due to the fact that in reactively coupled oscillators, the coupling force is related to the amplitude rather than the phase, and hence the phase trajectories of reactively coupled oscillators are modified when the oscillation frequency is a function of the oscillation amplitude [5,20]. In this case, the a - f correlation is increased by increasing V_F .

When V_F is set to 32 mV, we find that the oscillators lock to a single frequency for a certain range of applied dc voltages. The same set of measurements is repeated by operating the oscillators at different V_{dc_2} (15 and 20 V) and V_F (32–160 mV) voltages, while V_{dc_1} (15–35 V) is varied. The measured output power P_{out} of specific unsynchronized and synchronized states is shown in Fig. 2(a), while several frequency locking ranges are shown in Figs. 2(b) and 2(c) (see the Supplemental Material [14]).

In these plots, a clear enhancement in the synchronization region (frequency locking range) can be seen as the feedback voltage is increased from 50 to 160 mV. This is associated with the increasing amplitude dependence of the frequency response of the resonator, as can be seen from Fig. 1(c). These findings are in general agreement with the modeling results discussed in the Supplemental Material [14] and theoretical work conducted earlier on the dependence of the frequency pulling effect in reactively coupled oscillators with the observation of synchronization [20].

The constant phase difference of entrained oscillators is another important characteristic of synchronization which is often not reported [11–13]. This characteristic differentiates synchronization from forced excitation where the phase of the forced resonator follows the phase of an externally generated excitation force [5]. Assuming the phase responses of the oscillators are denoted as $\phi_1(t)$

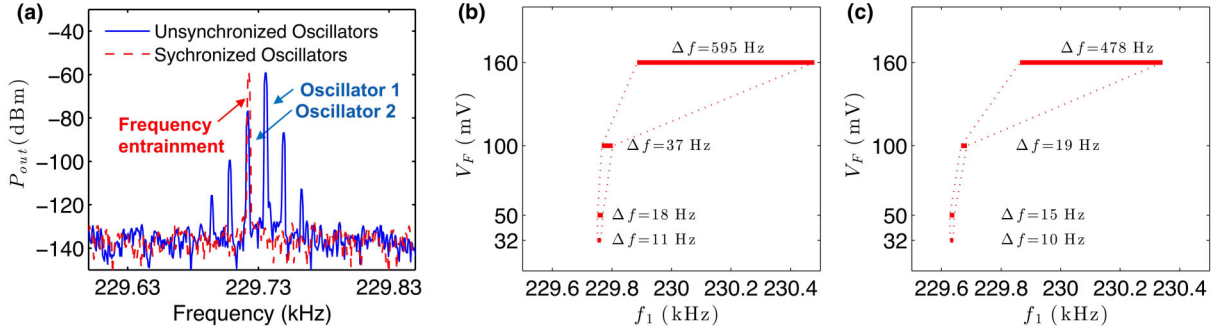


FIG. 2 (color online). Response of the coupled oscillators. (a) Two marked peaks are observed in the frequency spectrum corresponding to the different output frequencies of the unsynchronized oscillators, while in the case of synchronization, a single peak is observed, indicating an entrainment condition. (b) Various frequency locking ranges are shown when the oscillators are operated at V_F values ranging from 32 to 160 mV and at (b) 15 V and (c) 20 V V_{dc_2} voltages. Here, f_1 is the output frequency of oscillator 1, while Δf represents the frequency difference of the uncoupled oscillators.

and $\phi_2(t)$ while the phase difference between them is $\Delta\phi = \phi_1(t) - \phi_2(t)$, a state of synchronization is consistent with $\Delta\phi = \phi_c$. Here, ϕ_c is considered to be bounded rather than constant, as the noise sources in the oscillators may result in limited perturbation in the phase response.

The relative phase response of the coupled oscillators is logged using a dual channel universal counter (Agilent 53132A). During these measurements, V_{dc_2} is kept constant while V_{dc_1} is tuned to vary the frequency difference between the two oscillators. Subsequently, the measurements are repeated for different feedback voltages. In Fig. 3(a), several phase locked states are shown, each corresponding to a different value of V_F (see the Supplemental Material [14]). The reactive coupling between the oscillators allows for attraction or repulsion of the phase trajectories, resulting in in-phase and out-of-phase synchronization. Moreover, when the oscillators are synchronized, different initial frequency mismatches result

in different ϕ_c values [5]. However, in our case, the variation in Δf is limited by the minimum possible variation in V_{dc_1} which controls the output frequency of oscillator 1 and limits the number of observed phase locked states. Further, when the frequency detuning is on the edge of the locking range, a nearly bounded phase difference was observed for a very short period of time, followed by sudden jumps of 2π in $\Delta\phi$ as shown by curve *B* in Fig. 3(b), illustrating the phase slip phenomenon. However, with higher detuning, the phase difference grows continuously, indicating loss of synchronization, as shown in curves *C*, *D*, and *E*.

Typically, in an electronic oscillator, fluctuations in the amplitude trajectory are limited due to the employed amplitude limiting mechanism (such as automatic gain control circuitry). However, due to the absence of a limiting mechanism in the phase trajectory, any perturbations in the phase resulting from a stochastic process get accumulated

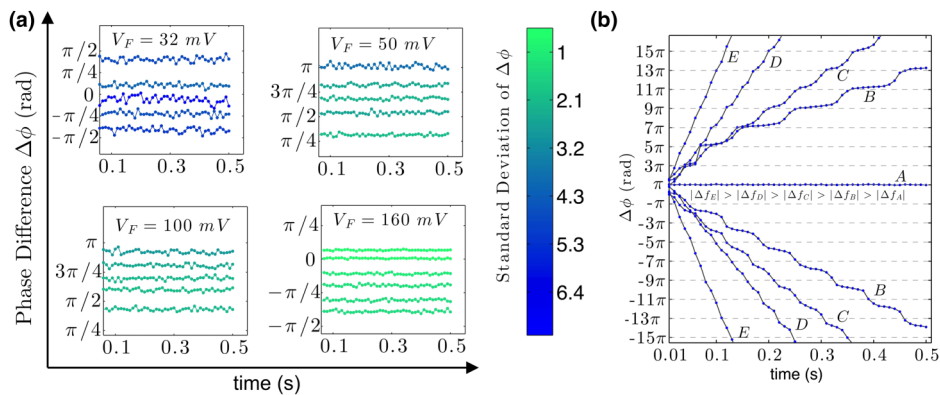


FIG. 3 (color online). Relative phase response ($\Delta\phi$) of synchronized and unsynchronized oscillators. (a) Several phase locked states are observed when the oscillators are operated at different values of V_F due to the variation in Δf and the initial phases. In these plots, the fluctuations in $\Delta\phi$ (in degrees) show the limited interaction of the inherent noise with the phase trajectories of each oscillator. A clear reduction of fluctuations in $\Delta\phi$ is observed with higher V_F voltages. (b) In this plot, curve *A* corresponds to an entrainment state while curve *B* demonstrates the phase slip phenomenon, indicating a state of nearly synchronized oscillators. As the frequency mismatch increases, the oscillators oscillate with the different frequencies, resulting in uniform boundless growth in $\Delta\phi$ (curves *C*, *D*, and *E*).

over time. These random fluctuations in phase, referred to as phase diffusion, often limit the stability of the oscillator output frequency [21]. Other factors such as environment sensitivity and component aging may induce drift in the output frequency [22].

In our experiments, for the synchronized case, we observe a reduction in the relative phase diffusion with higher V_F values, as shown in Fig. 3(a). A high V_F increases the correlation between amplitude and phase responses as discussed, and hence the impact of the coupling force on the phases of the coupled oscillators is increased. Thus, the coupling force acts as a phase control mechanism to reduce random phase fluctuations when the oscillators are synchronized. However, it has been independently observed that the higher cubic nonlinearity of the MEMS resonator may degrade the frequency stability of the oscillator [23,24]. Therefore, to compare the frequency fluctuations of the uncoupled oscillators with the synchronized case, we must determine the optimum feedback voltage at which the uncoupled oscillators demonstrate the greatest frequency stability.

A comparison of the frequency stability can be carried out using the nonoverlapping estimation of the Allan deviation [$\sigma_y(\tau)$] at various integration times (τ) from the sampled time history [25]. To calculate $\sigma_y(\tau)$ of the implemented oscillators, the output frequencies of the uncoupled oscillators is logged using a frequency counter for 600 s with a sampling time of 0.2 s at different values of V_F , and the recorded data are averaged over different integration times. Subsequently, the frequency response of the synchronized oscillators is recorded. Using the measured frequency response of the uncoupled oscillators, the calculated Allan deviation of oscillator 2 is shown in Fig. 4(a). From these plots, it can be seen that at a V_F of 50 mV, frequency fluctuations are the least, and this is also the case for oscillator 1. At this driving voltage, $\sigma_y(\tau)$ of the synchronized oscillator 2 is shown in Fig. 4(b). In these plots, a clear improvement in the frequency stability can be seen when the oscillators are synchronized.

A similar improvement is observed for oscillator 1 (see the Supplemental Material [14]). In these plots, the negative, zero, and positive slope responses indicate the presence of white, $1/f$, and random walk frequency noise sources in the oscillator [26].

In these measurements, we observe an improvement in the short-term frequency stability of the synchronized oscillator 2 ($\tau = 0.2$ s) by a factor of $\approx 7\times$ compared to the uncoupled case. Thus, the phase locking characteristic inherent to the synchronization process can be used as a frequency stabilization mechanism to improve the frequency stability of MEMS oscillators. Moreover, this observation challenges existing theories which predict that the improvement in the frequency stability of synchronized oscillators scales only as the number of oscillators in the array [27,28]. Our results demonstrating $\approx 7\times$ improvement in the short-term frequency stability in a two element array of coupled oscillators indicate that this enhancement in frequency stability may be more significant than previously predicted. These observations open the door to further studies and the engineering of the phenomenon of synchronization to applications in miniaturized timing devices and frequency references.

In this Letter, we report a minimum frequency fluctuation (for the unsynchronized case) when the oscillators are operated at a V_F of 50 mV. However, random fluctuations in the phase difference of the synchronized oscillators were found to be least at a V_F of 160 mV. This discrepancy may be due to the cross correlation between amplitude and phase noise, modulated by V_F due to displacement-dependent resonator nonlinearities. Therefore, an increase in V_F may increase the random perturbations in the phase trajectories of the individual oscillators [29]. If the coupling force between the phase trajectories can be suitably increased without changing the nonlinear dynamics of the MEMS oscillators, a further improvement in frequency stability may be achieved.

This Letter presents the first experimental realization of electrostatically driven coupled micromechanical

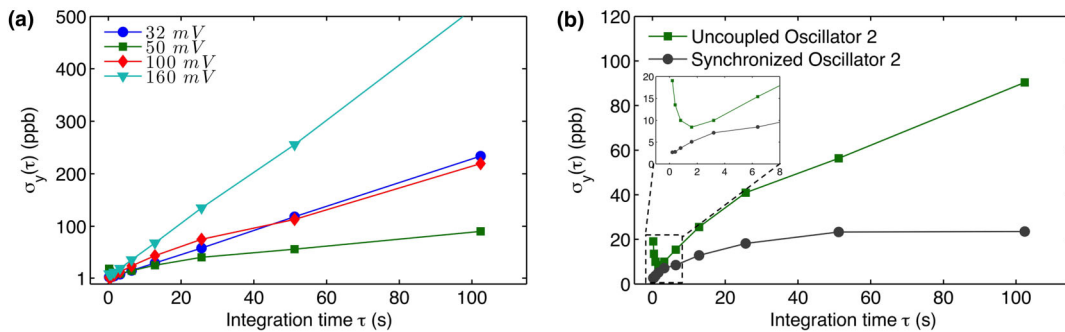


FIG. 4 (color online). Allan deviation [$\sigma_y(\tau)$] of the implemented MEMS oscillators. (a) A nonoverlapping estimation of $\sigma_y(\tau)$ of the uncoupled oscillator 2 is shown here in units of parts per billion (ppb) with respect to various integration times. A trade-off between V_F and $\sigma_y(\tau)$ can be observed in these plots due to the dependency of the output signal power and the a - f correlation on V_F . (b) $\sigma_y(\tau)$ of the oscillator for uncoupled and synchronized cases are compared here. In both the cases, the oscillator is operated at a V_F of 50 mV. A clear enhancement in the frequency stability is visible when the oscillator is entrained, compared to the uncoupled case.

oscillators where several different states of synchronization are reported associated with reduction in the combined phase diffusion rate. The employed coupling could also be implemented in electronic oscillators based on other technologies. Furthermore, the presented methodology can conceptually be scaled to larger-scale arrays, providing a test bed for studies on the dynamics of coupled synchronized oscillators in the presence of nonlinearities and stochastic processes. These investigations could lead to the realization of practical applications in information processing [6,7] and timing references [8–10].

The authors acknowledge financial support from the UK-India Educational and Research Initiative (Grant No. SA06-250) and the Cambridge Commonwealth Trust.

*Corresponding author.

aas41@cam.ac.uk

- [1] C. Huygens, *Horologium Oscillatorium* (Apud F. Muguet, Paris, France, 1673).
- [2] M. Bennett, M.F. Schatz, H. Rockwood, and K. Wiesenfeld, *Proc. R. Soc. A* **458**, 563 (2002).
- [3] J. Simonet, M. Warden, and E. Brun, *Phys. Rev. E* **50**, 3383 (1994).
- [4] J. Buck and E. Buck, *Science* **159**, 1319 (1968).
- [5] A. Pikovsky, M. Rosenblum, and J. Kurths, *Synchronization: A Universal Concept in Nonlinear Sciences* (Cambridge University Press, Cambridge, England, 2001).
- [6] I. Mahboob and H. Yamaguchi, *Nat. Nanotechnol.* **3**, 275 (2008).
- [7] T. Nishikawa, Y.C. Lai, and F.C. Hoppensteadt, *Phys. Rev. Lett.* **92**, 108101 (2004).
- [8] C. T.-C. Nguyen, *IEEE Trans. Ultrason. Ferroelectr. Freq. Control* **54**, 251 (2007).
- [9] X.L. Feng, C.J. White, A. Hajimiri, and M.L. Roukes, *Nat. Nanotechnol.* **3**, 342 (2008).
- [10] D. Antonio, D.H. Zanette, and D. Lopez, *Nat. Commun.* **3**, 806 (2012).
- [11] S.-B. Shim, M. Imboden, and P. Mohanty, *Science* **316**, 95 (2007).
- [12] M. Zalalutdinov, K. Aubin, M. Pandey, A. Zehnder, R. Rand, H. Craighead, J. Parpia, and B. Houston, *Appl. Phys. Lett.* **83**, 3281 (2003).
- [13] M. Zhang, G.S. Wiederhecker, S. Manipatruni, A. Barnard, P. McEuen, and M. Lipson, *Phys. Rev. Lett.* **109**, 233906 (2012).
- [14] See Supplemental Material at <http://link.aps.org/supplemental/10.1103/PhysRevLett.111.084101> for additional information on theoretical modeling and additional experimental data.
- [15] C.T.-C. Nguyen and R.T. Howe, *IEEE J. Solid-State Circuits* **34**, 440 (1999).
- [16] E. Buks and M. Roukes, *J. Microelectromech. Syst.* **11**, 802 (2002).
- [17] M. Agarwal, K.K. Park, R.N. Candler, M.A. Hopcroft, C.M. Jha, R. Melamud, B. Kim, B. Murmann, and T.W. Kenny, in *IEDM Technical Digest: Proceedings of the Electron Devices Meeting, Washington, DC, 2005* (IEEE, New York, 2005), p. 295.
- [18] D.E. Newland, *Mechanical Vibration Analysis and Computation* (Longman Scientific and Technical, Harlow, 1989).
- [19] J.E.-Y. Lee, B. Bahreyni, Y. Zhu, and A.A. Seshia, *IEEE Electron Device Lett.* **29**, 701 (2008).
- [20] M.C. Cross, A. Zumdieck, R. Lifshitz, and J.L. Rogers, *Phys. Rev. Lett.* **93**, 224101 (2004).
- [21] A. Hajimiri and T.H. Lee, *IEEE J. Solid-State Circuits* **33**, 179 (1998).
- [22] J. Rutman, *Proc. IEEE* **66**, 1048 (1978).
- [23] P. Ward and A. Duwel, *IEEE Trans. Ultrason. Ferroelectr. Freq. Control* **58**, 195 (2011).
- [24] H.K. Lee, P.A. Ward, A.E. Duwel, J.C. Salvia, Y.Q. Qu, R. Melamud, S.A. Chandorkar, M.A. Hopcroft, B. Kim, and T.W. Kenny, in *Proceedings of the 16th Solid-State Sensors, Actuators, and Microsystems Conference, Beijing, 2011* (IEEE, New York, 2011), p. 510.
- [25] W.D. Allan, *Proc. IEEE* **54**, 221 (1966).
- [26] E. Rubiola, *Phase Noise and Frequency Stability in Oscillators* (Cambridge University Press, Cambridge, England, 2009).
- [27] N. Masuda, Y. Kawamura, and H. Kori, *New J. Phys.* **12**, 113002 (2010).
- [28] M.C. Cross, *Phys. Rev. E* **85**, 046214 (2012).
- [29] B. Yurke, D.S. Greywall, A.N. Pargellis, and P.A. Busch, *Phys. Rev. A* **51**, 4211 (1995).